

Real-Time Estimation* of Local Atmospheric Density[†]

James R. Wright[‡]

Abstract

A method is presented for the real-time estimation of atmospheric density, locally along the trajectory of a low altitude spacecraft. Atmospheric density is estimated simultaneously with six parameters of the spacecraft orbit, and with other parameters that are both observable and unknown. Atmospheric density is derived by estimating local corrections directly to a global atmospheric density model. These corrections are derived, in part, from real-time range and/or Doppler tracking data. They are also derived from $F_{10.7}$ and a_P measurement values. $F_{10.7}$ and a_P measurements are used conventionally to drive the global atmospheric density model. But they are also employed by two new *stochastic* atmospheric density *error* models: A baseline error model and a dynamic error model. The baseline error model is derived from the historical record of $F_{10.7}$ and a_P measurements across multiple eleven year solar cycles. The dynamic error model is an extension to the baseline model, and is derived from current $F_{10.7}$ and a_P measurements. This provides a new physical connection between the physics of atmospheric density and atmospheric density estimation. *Real-time* here means that the time-lag for estimation of the local atmospheric density is less than one second following the arrival of new range and/or Doppler tracking data. Atmospheric density estimation is demonstrated with real LEO tracking data acquired during July 2000 – at solar maximum.

1 Introduction

A method is presented for the real-time estimation of atmospheric density, locally along the trajectory of a low altitude spacecraft. Atmospheric density is estimated simultaneously with six parameters of the spacecraft orbit, and with other parameters that are both observable and unknown. Atmospheric density is derived by estimating local atmospheric density corrections to a global atmospheric density model. These corrections are derived, in part, from real-time range and/or Doppler tracking data. They are also derived from $F_{10.7}$ and a_P measurement values. $F_{10.7}$ and a_P measurements are used conventionally to drive the global atmospheric density model. But they are also employed here by two new *stochastic* atmospheric density *error* models: A baseline error model and a dynamic error model.

Let ρ denote atmospheric density, and $\bar{\rho}$ an estimate of ρ derived from a global a priori atmospheric density model. Define $\Delta\rho = \rho - \bar{\rho}$ the error in $\bar{\rho}$, $\Delta\hat{\rho}$ a real-time estimate of $\Delta\rho$, and $\hat{D} = \Delta\hat{\rho}/\bar{\rho}$.

1.1 Baseline Atmospheric Density Error Model

The baseline error model is derived from the *historical record* of F_{10} and a_P measurements across multiple eleven year solar cycles. An exponential Gauss-Markov sequence is employed to propagate relative atmospheric density error estimates \hat{D} at perigee height, and to add appropriate baseline error process noise variance $q_{\Delta\rho/\bar{\rho}}$ for propagations during quiet solar weather. In the absence of measurements the relative atmospheric density error variance $\sigma_{\Delta\rho/\bar{\rho}}^2$ is a time constant (stationary). But during the processing of each observable measurement, $\sigma_{\Delta\rho/\bar{\rho}}^2$ is reduced (i.e., $\sigma_{\Delta\rho/\bar{\rho}}^2$ is non-stationary during measurement processing).

A transformation is defined to relate the atmospheric density error estimate at perigee height to that at current spacecraft height.

*© Analytical Graphics, Inc. 2003. Publication permission granted to AAS/AIAA.

[†]This method is the subject of a current U.S. patent application by Analytical Graphics, Inc.

[‡]Senior Engineer, Analytical Graphics, Inc.

1.2 Dynamic Atmospheric Density Error Model

The dynamic error model is an extension to the baseline model. It simultaneously invokes the atmospheric density due to *current* $F_{10.7}$ and a_P measurements, and the atmospheric density due to global *mean* values of $F_{10.7}$ and a_P measurements, to form a scaling ratio R . The scaling ratio is used to boost the baseline error variance $\sigma_{\Delta\rho/\bar{\rho}}^2$ to derive $Q_{\Delta\rho/\bar{\rho}} = R^2\sigma_{\Delta\rho/\bar{\rho}}^2$ dynamically. With every significantly increasing sequence of atmospheric density $\bar{\rho}$ at perigee height, the relative atmospheric density error $\Delta\rho/\bar{\rho}$ is modeled as a modified random walk sequence. When the increasing sequence is terminated, the relative atmospheric density error variance propagation returns to baseline Gauss-Markov propagation. The rate of return is defined by the density of range and/or Doppler tracking measurements processed, and by exponential half-life of the Gauss-Markov sequence. This provides a new physical connection between the physics of atmospheric density and atmospheric density estimation.

The dynamic error model is particularly useful during solar maximum with volatile increasing measurements of $F_{10.7}$ and a_P that predict associated increases in atmospheric density and atmospheric density error magnitude. This enables the error process noise variance $Q_{\Delta\rho/\bar{\rho}}$, and the sequential filter gain on atmospheric density error $\Delta\rho/\bar{\rho}$, to be opened appropriately at exactly the right time.

1.3 Real-Time

The new method is distinguished from existing and previous methods in that atmospheric density error correction $\Delta\hat{\rho}/\bar{\rho}$ is estimated directly in *real-time*, in association with optimal sequential orbit determination [11]. *Real-time* here means that the time-lag for estimation of the local atmospheric density is less than one second following the arrival of new tracking data¹. This performance is, of course, impossible using batch least squares techniques.

1.4 Real Data Results

The Bastille Day geomagnetic storm began with a solar flare and solar coronal mass ejection (CME) on 14 July 2000 that was observed by the SOHO spacecraft coronagraph (J. Burch[15]). The CME slammed into the earth late on 15 July 2000, accompanied by a sharp decrease (-300 nanoteslas) in the strength of the geomagnetic field at the earth's surface. And a_P rose to 400 ($\max a_P$). We acquired real range tracking data covering the interval from 1 July 2000 through 26 July 2000 for two near-circular LEO spacecraft *LEO*h497 and *LEO*h780. Spacecraft heights were roughly $497km$ and $780km$ respectively. According to Tom Gidlund [18], the estimation of ballistic coefficient time-constants using least squares orbit determination, for these LEOs, presented significant orbit determination problems during that time at solar maximum.

The results of both sequential filtering and sequential smoothing are presented for time-varying atmospheric density estimation for *LEO*h497 and *LEO*h780. The times of significant corrections to atmospheric density, due to both direct solar radiation and geomagnetic disturbances, are shown to be in agreement with the effective lags, 1.70^d for $F_{10.7}$ and 0.279^d for K_P , expected by the Jacchia 1971 (J71) global atmospheric density model[1].

1.5 Minimization of Orbit Error Magnitudes

The new method should prove to be useful for minimization of orbit error magnitudes for real-time and predicted LEO spacecraft trajectories. This is due to the use of an optimal orbit determination method[11], where the local time-varying atmospheric density modeling error is appropriately absorbed by the local time-varying atmospheric density error estimate. Otherwise atmospheric density error would be aliased into correlated orbit states (mean motion and mean longitude most significantly), thereby degrading the orbit estimate.

Least squares orbit determination methods minimize the sum of squares of measurement residuals, not orbit error magnitudes. And least squares methods estimate a ballistic coefficient time

¹The term *near real-time* has been used recently to refer to a time-lag of up to eight hours. Were it not for this, I would have used *near real-time* in place of *real-time*.

constant, not the local time varying atmospheric density. It is thus not surprising that least squares methods frequently do not estimate atmospheric density errors in response to significant increases in a_P (see Owens[10]). Unestimated atmospheric density modeling errors are unfortunately aliased into the least squares orbit estimate.

1.6 Predictions

The new method employs a serially correlated stochastic sequence, a Gauss-Markov model, to represent atmospheric density estimates. These time-varying estimates are derived from range and/or Doppler tracking measurements by the filter measurement update function. They are predicted forward by the filter time update function. And they are returned to zero exponentially with time, according to the half-life specified for the Gauss-Markov model.

There are at least two sources of air-drag acceleration error, an error in atmospheric density and an error in the ballistic coefficient (see Eq. 10). Both errors must be estimated and thereby removed. Given the technique identified below to estimate and remove the observable part of any constant mean ballistic coefficient, an optimal predicted estimate of the local atmospheric density is achieved.

This is in sharp contrast to the use of an estimated time-constant ballistic coefficient for least squares predictions, while ignoring the time-varying error in atmospheric density.

2 Global Atmospheric Density Model

A global atmospheric density model refers to a capability to model atmospheric density at any LEO position and time, whether past, current, or in the future. Global models are driven deterministically by $F_{10.7}$ and a_P (or K_P) measurement values. Global atmospheric density estimates are accompanied by significant atmospheric density modeling errors.

LEO least squares orbit determination programs use global atmospheric models, and estimate local ballistic coefficient *time constants* in an effort to absorb the effect of *time-varying* atmospheric density modeling errors. For least squares this is necessary, but it is far from optimal. Atmospheric density modeling errors are time variable, not time constant, and during solar maximum relative error magnitudes can, and do, exceed 100% (see the filter-smoother results presented herein).

2.1 Jacchia 1971

The Jacchia 1971 (J71) global atmospheric density model[1] was adopted in 1972 as the COSPAR international Reference Atmosphere (CIRA72)[2]. It models atmospheric density ρ from a lower height of 110 km to an upper height of 2000 km, referred to the earth's surface. J71 has been used operationally for thirty years. I have selected it for use in the real-time estimation of atmospheric density.

2.1.1 K_P vs a_P

K_P and a_P are used interchangeably in the literature on atmospheric density modeling. K_P and a_P refer to the same geomagnetic measurement information, and can be related² approximately with the empirical nonlinear transformation (compare Eqs. 21 and 22 from J70 [3]):

$$28^\circ K_P + 0.03^\circ \exp(K_P) = 1.0^\circ a_P + 100^\circ [1 - \exp(-0.08a_P)]$$

² K_P is a three-hour average of irregular geomagnetic range disturbances in two horizontal field components (H and D), measured at thirteen mid-latitude stations by ground based magnetometers. At a particular station, the natural logarithm of the largest excursion in H or D over a three hour period is recorded on a scale from 0 to 9. K_P measurements are defined only at thirds of each unit (e.g., 0, 1/3, 2/3, 3/3), where $0 \leq K_P \leq 9$. a_P was defined to present geomagnetic range disturbances on a linear scale, as a table of transformed values $0 \leq a_P \leq 400$, with a one-to-one discreet mapping with K_P , and boundaries defined by $(K_P = 0) \Leftrightarrow (a_P = 0)$, and $(K_P = 9) \Leftrightarrow (a_P = 400)$. The transformation given by $F(K_P, a_P)$ provides a continuous map between K_P and a_P , but where $(K_P = 0) \Leftrightarrow (a_P = 0)$ is not satisfied exactly.

where the temperature unit is in degrees Kelvin. Rearrange the equation above to define the non-linear function $F(K_P, a_P)$:

$$F(K_P, a_P) = \{1.0^\circ a_P + 100^\circ [1 - \exp(-0.08a_P)]\} - \{28^\circ K_P + 0.03^\circ \exp(K_P)\}$$

where:

$$F(K_P, a_P) = 0$$

Given a value for K_P (or a_P), then solve the function $F(K_P, a_P)$ for a_P (or K_P) iteratively (e.g., with Newton-Raphson). Although this seems a trivial matter, it is necessary to be able to discuss K_P and a_P interchangeably.

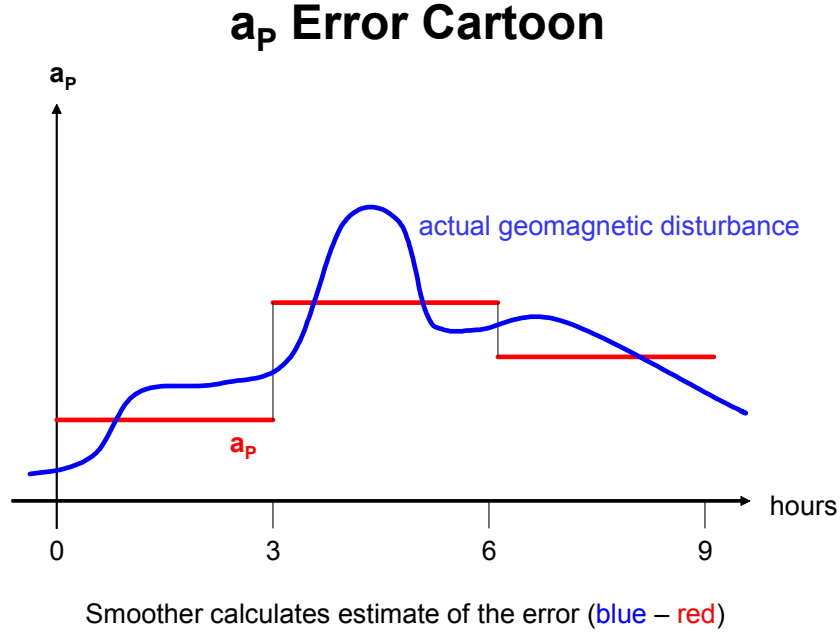


Figure 1: Geomagnetic Disturbance vs a_P

2.1.2 $F_{10.7}$, $\bar{F}_{10.7}$ and K_P (or a_P) in J71

$F_{10.7}$ is the 10.7cm daily solar flux, a daily average of measured values, reported daily. $\bar{F}_{10.7}$ is an average of $F_{10.7}$ over six solar rotations, reported daily. $F_{10.7}$ measures particular active regions of the solar disk, but $\bar{F}_{10.7}$ is associated with the entire solar disk. Measured values of the geomagnetic index K_P are averaged across three hour intervals to provide a single K_P (and a_P) constant for each three hour interval. Atmospheric density is extremely sensitive to realizable variations in input values for K_P and $F_{10.7}$, according to J71 [1]. Atmospheric temperatures define the bridge between K_P and $F_{10.7}$ measurement values and atmospheric density. From Jacchia Eq. 14:

$$T_c = 379^\circ + 3.24^\circ \bar{F}_{10.7} + 1.3^\circ (F_{10.7} - \bar{F}_{10.7}), \quad \text{for } K_P = 0 \quad (1)$$

where T_c (degrees Kelvin) denotes the night time minimum of the global asymptotic exospheric temperature T_∞ for $K_P = 0$ (and $a_P = 0$). T_∞ is a function of T_c , then T_∞ is augmented with K_P information according to Jacchia Eq. 18:

$$\Delta T_\infty = 28^\circ K_P + 0.03^\circ \exp(K_P) \quad (2)$$

Then T_∞ drives the calculation of atmospheric density ρ .

Thus according to Jacchia, atmospheric density is driven by both $F_{10.7}$ and K_P . Correlations between ρ , T_∞ , $\bar{F}_{10.7}$, $F_{10.7}$, and K_P are presented graphically in Jacchia Figures 6 and 7 [1].

And according to Jacchia, the effect of changes of $F_{10.7}$ on the atmosphere lags the $F_{10.7}$ measurement time by 1.7 days (40.8 hours). And the effect of changes in the K_P measurement on the atmosphere lags the K_P measurement time by 0.279 days (6.7 hours). Given current values for $F_{10.7}$ and K_P , these lags provide *predictive power* for real-time atmospheric density estimation and for real-time orbit determination.

3 Global Atmospheric Density Modeling Errors

3.1 Constants and Discontinuities in a_P

On 15 July 2000, values for a_P did jump from 32 over the interval $(9^h, 12^h)$ to 207 at 12^h for the interval $(12^h, 15^h)$. These a_P values are given as constants across three hour time intervals. But in fact the discontinuity at 12^h is fictitious, and it generates a huge error in the value for atmospheric density ρ calculated by J71. Another huge error in ρ is incurred because the actual profile of geomagnetic disturbance with time is absent across each three-hour a_P interval. The a_P peak variation magnitude is obviously significantly larger than any average. It is useful to view a sequence of a_P three-hourly values beginning at nine hours on 15 July 2000: $\{\dots, 32, 207, 300, 400, 300, 179, 80, 32, \dots\}$, a sequence that invokes huge modeling errors correlated in part with discontinuities between the three-hour constants. I treat all increasing sequences in a_P as modified random walk functionals. That is, given the value $a_P = a_P(t, t + 3h)$, then define the predicted estimate \hat{a}_P :

$$\hat{a}_P(t + 3h, t + 6h) = a_P(t, t + 3h)$$

Then the error $\delta a_P(t + 3h, t + 6h)$ in $\hat{a}_P(t + 3h, t + 6h)$ is given by:

$$\begin{aligned} \delta a_P(t + 3h, t + 6h) &= a_P(t + 3h, t + 6h) - \hat{a}_P(t + 3h, t + 6h) \\ &= a_P(t + 3h, t + 6h) - a_P(t, t + 3h) \end{aligned}$$

This generates a realistic mechanism for modeling errors due to discontinuities in a_P between the three-hourly time constants in a_P . These errors map to evaluations of atmospheric density ρ according to Eq. 2.

The cartoon defined by Fig. 1 presents a fictitious explanatory example: Let d denote the difference between actual geomagnetic disturbance and a_P . For those times between discontinuities in a_P , d is a continuous function because both the geomagnetic disturbance and a_P are continuous functions. But at each discontinuity in a_P , the difference d is also discontinuous. Then given real-time range tracking data that measures the actual geomagnetic disturbance, one should expect that the sequentially smoothed corrections to modeled atmospheric density would present continuous functions between discontinuities in a_P , but would present discontinuities at the times of discontinuities in a_P . Also, this cartoon suggests the existence of both negative and positive values in the difference d . Thus one should also expect both negative and positive values in the smoothed corrections to modeled atmospheric density. Actual variations of the smoothed atmospheric density estimation results presented herein are thus explained, and an important necessary condition for validation of the method is established.

During quiet geomagnetic weather the maximum values of a_P are smaller than at solar maximum, and the three-hourly variation magnitudes in a_P are also smaller. Consequently the associated values of ρ at fixed spacecraft height are smaller than at solar maximum, and variation magnitudes in ρ at fixed spacecraft height are also smaller. But during solar maximum the maximum values of a_P are large, and the three-hourly variation magnitudes in a_P are also large. Consequently the associated values of ρ at fixed height are relatively large, and variation magnitudes in ρ at fixed height are also large.

3.2 Constants and Discontinuities in $F_{10.7}$

A similar phenomenon exists with the daily mean values of $F_{10.7}$. I treat increasing daily mean value sequences of $F_{10.7}$ as modified random walk functionals. During quiet solar weather the maximum values of $F_{10.7}$ are relatively small, and the daily variation magnitudes in $F_{10.7}$ are also small. Consequently the associated values of ρ at fixed spacecraft height are relatively small, and variation magnitudes in ρ at fixed spacecraft height are also small. But during solar maximum the maximum values of $F_{10.7}$ are large, and the daily variation magnitudes in $F_{10.7}$ are also large. Consider the sequence beginning with 6 July 2000: $\{\dots, 174, 187, 210, 211, 244, 241, 315, 232, 204, 213, 219, 228, \dots\}$. Consequently the associated values of ρ at fixed spacecraft height are relatively large, and variation magnitudes in ρ at fixed spacecraft height are also large.

3.3 Estimation Errors in Global Models

A review of the development of J71 [1][2] reveals the source of significant atmospheric density modeling errors that are independent of discontinuities in $F_{10.7}$ and a_P .

4 Adopted Principles

4.1 The Fixed-Height Principle

A mechanism is required to increase the filter baseline error variance σ_ρ^2 on atmospheric density due to the effects of significant increases in $F_{10.7}$, $\bar{F}_{10.7}$ and a_P , particularly during solar maximum. This requirement derives especially from the use of time constants and discontinuities in $F_{10.7}$ and a_P discussed above. For fixed spacecraft height, I identify a *fixed height principle* between atmospheric density ρ and its error variance σ_ρ^2 : A significant increase in atmospheric density ρ , at fixed spacecraft height, implies a significant increase in estimated atmospheric density error variance σ_ρ^2 at that height.

4.1.1 A Simple Experiment with Height Variations Using J71

The *fixed height principle* suggests the need for a definition for mean atmospheric density derived from mean values $\langle F_{10.7} \rangle$, $\langle \bar{F}_{10.7} \rangle$, and $\langle a_P \rangle$ for comparison to current atmospheric density derived from current values of $F_{10.7}$, $\bar{F}_{10.7}$ and a_P , all at fixed spacecraft height. But the *fixed height principle* leads to a surprising result. The description of the simple experiment that follows illuminates this result.

I have selected $\langle F_{10.7} \rangle = \langle \bar{F}_{10.7} \rangle = 150$ and $\langle a_P \rangle = 20$ as mean values for $F_{10.7}$, $\bar{F}_{10.7}$ and a_P across multiple eleven year solar cycles. Associate density $\langle \rho(h) \rangle$ with $\langle F_{10.7} \rangle$, $\langle \bar{F}_{10.7} \rangle$, and $\langle a_P \rangle$. Evaluate atmospheric density at spacecraft heights $h = 497km$ and $h = 780km$, for mean values $\langle F_{10.7} \rangle$, $\langle \bar{F}_{10.7} \rangle$, $\langle a_P \rangle$, and for³ $F_{10.7} = 213$ and $a_P = 400$. Denote the density function $\rho = \rho(h, F_{10.7}, \bar{F}_{10.7}, a_P)$, and define the ratio:

$$\mathbf{Ratio} = R(h, F_{10.7}, \bar{F}_{10.7}, a_P) = \frac{\rho(h, F_{10.7}, \bar{F}_{10.7}, a_P)}{\langle \rho(h) \rangle} \quad (3)$$

Then evaluate the ratio of densities at each height using J71:

Then for $F_{10.7} = 213$ and $a_P = 400$ on 15 July 2000, referred to mean values $\langle F_{10.7} \rangle$ and $\langle a_P \rangle$, the density is increased by a factor of five at $h = 497km$, but is increased by a factor of seventeen at $h = 780km$. This is an example of a general property that I shall refer to as the *ratio-height principle*.

³At 18 hours on 15 July 2000, the record shows $F_{10.7} = 213$ and $a_P = 400$. July 2000 was at solar maximum, and the explosion in a_P was due to earth impact of a coronal mass ejection.

h (km)	$F_{10.7}$	a_P	ρ (kg/m ³)	Ratio
497	150	20	1.1×10^{-12}	5
497	213	400	5.9×10^{-12}	
780	150	20	2.6×10^{-14}	
780	213	400	4.3×10^{-13}	17

Table 1: Height Dependent Density Ratios

4.2 The Ratio-Height Principle

The *Ratio Height Principle*: The ratio of atmospheric density during solar maximum to mean atmospheric density, both at the same height, increases significantly when spacecraft height is increased.

5 Baseline Model for Atmospheric Density Error Variance

Define:

$$\sigma_{\Delta\rho/\bar{\rho}}(h) = \sqrt{E \left\{ \left(\frac{\Delta\rho(h)}{\bar{\rho}(h)} \right)^2 \right\}} = \frac{\sqrt{E \{ (\Delta\rho(h))^2 \}}}{\bar{\rho}(h)} = \frac{\sigma_{\Delta\rho}(h)}{\bar{\rho}(h)} \quad (4)$$

where:

$$\Delta\rho(h) = \rho(h) - \bar{\rho}(h) \quad (5)$$

where $\rho(h)$ is true atmospheric density at height h (in km), and $\bar{\rho}(h)$ is the associated value of estimated atmospheric density according to J71. The *baseline error variance model* was derived as a height dependent function by evaluating first and second moments on relative atmospheric errors across multiple solar cycles. An estimated graph of the root-variance $\sigma_{\Delta\rho/\bar{\rho}}(h)$ is presented by Figure 2.

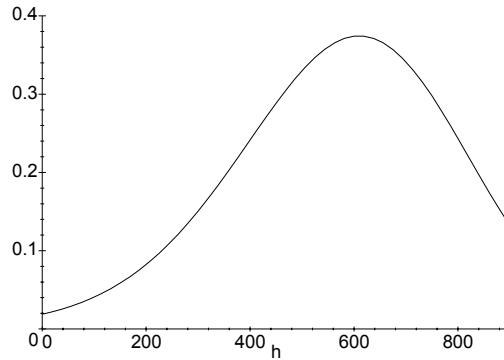


Figure 2: Sigma for Relative Error in Air Density

The ordinate displays $\sigma_{\Delta\rho/\bar{\rho}}(h)$ as a function of spacecraft height h in kilometers. Denote this graph with the function:

$$f(h) = \sigma_{\Delta\rho/\bar{\rho}}(h) \quad (6)$$

Then $f(h)$ can be sampled simultaneously at two heights, say h at current spacecraft height and h_P at orbit perigee height, to define a ratio $f(h)/f(h_P)$ of relative atmospheric density error in terms of averages across multiple solar cycles:

$$\frac{f(h)}{f(h_P)} = \frac{\sigma_{\Delta\rho/\bar{\rho}}(h)}{\sigma_{\Delta\rho/\bar{\rho}}(h_P)} = \frac{\sigma_{\Delta\rho}(h)/\bar{\rho}(h)}{\sigma_{\Delta\rho}(h_P)/\bar{\rho}(h_P)} \quad (7)$$

See Eq. 4.

6 Air Drag Acceleration Error Model

The perturbative air-drag acceleration \ddot{z}_D has the form:

$$\ddot{z}_D = -\frac{1}{2}B\rho\hat{s}^2K, \quad B = \frac{C_D A}{m} \quad (8)$$

where \ddot{z}_D is a 3×1 perturbative drag acceleration matrix with inertial components, C_D is the unitless drag coefficient, A is the spacecraft area projection onto a plane orthogonal to the spacecraft velocity vector $\hat{\mathbf{s}}$ referred to a rotating Earth, \hat{s} is the length of $\hat{\mathbf{s}}$, m is spacecraft mass, ρ is atmospheric density, and K is a 3×1 unit matrix that contains inertial components of $\hat{\mathbf{s}}/\hat{s}$.

Differentiate Eq. 8 to derive random errors in \ddot{z}_D from random errors in C_D , A , ρ , and m :

$$\Delta\ddot{z}_D = \left(\frac{\Delta C_D}{C_D} + \frac{\Delta A}{A} + \frac{\Delta\rho}{\rho} - \frac{\Delta m}{m} \right) \ddot{z}_D \quad (9)$$

Suppose $\Delta C_D/C_D$, $\Delta A/A$, $\Delta m/m$, and $\Delta\rho/\rho$ are all unknown. If they are observable, optimal orbit determination[11] would generate useful estimates of all four parameters. Typically, they are not all observable. But if there exists a useful mean value of B that is a time constant, then the differentiation of Eq. 8 provides:

$$\Delta\ddot{z}_D = \left(\frac{\Delta B}{B} + \frac{\Delta\rho}{\rho} \right) \ddot{z}_D \quad (10)$$

noting that $\Delta\rho/\rho = \Delta\rho(t)/\rho(t)$ is always time variable. If one has sufficient tracking data to observe both $\Delta B/B$ and $\Delta\rho/\rho$, then one could estimate them simultaneously. But for now I shall take a different approach.

Denote $D(t) = \Delta\rho(t)/\rho(t)$. If one at first sequentially estimates only $D(t)$, and not $\Delta B/B$, using a biased a priori estimate \bar{B} in Eq. 8, and ignores the error $\Delta B = B - \bar{B}$ in \bar{B} , then the estimated sequence $\bar{D}(t) = D(t) - \Delta D$ will produce a biased graph. Then modify the a priori estimate \bar{B} experimentally so as to generate an unbiased graph $\hat{D}(t)$, and an associated estimate $\Delta\hat{B}$, where $\hat{B} = \bar{B} + \Delta\hat{B}$. Henceforth use \hat{B} in Eq. 8. Then one derives unbiased estimates for the sequence $D(t) = \Delta\rho(t)/\rho(t)$ because useful mean values of B and ΔB are time constants and the bias ΔB has been removed. How shall we model $D(t)$?

7 Gauss-Markov Sequence

Define:

$$D(t) = \frac{\Delta\rho_{h_P}(t)}{\bar{\rho}_{h_P}(t)} \quad (11)$$

at mean perigee height h_P , where $D(t)$ satisfies the equation:

$$D(t_{k+1}) = \Phi(t_{k+1}, t_k) D(t_k) + \sqrt{1 - \Phi^2(t_{k+1}, t_k)} w(t_k) \quad , \quad k \in \{0, 1, 2, \dots\} \quad (12)$$

where $w(t)$ is a Gaussian white random variable with mean zero and variance σ_w^2 , where:

$$D(t_0) = w(t_0) \quad (13)$$

$$\Phi(t_{k+1}, t_k) = e^{\alpha|t_{k+1} - t_k|} \quad (14)$$

$$\text{constant } \alpha < 0 \quad (15)$$

$$\sigma_{\Delta\rho/\bar{\rho}}^2(t_k) = E \{D^2(t_k)\}, \text{ for each } k, \quad (16)$$

and where $D(t_k)$ is Gauss-Markov, and:

$$\sigma_{\Delta\rho/\bar{\rho}}^2(t_k) = E \{D^2(t_k)\} = \sigma_w^2, \text{ for each } k \quad (17)$$

Variance $\sigma_{\Delta\rho/\bar{\rho}}^2(t_k)$ varies significantly with height h . Thus it is necessary to choose a height for $\Delta\rho/\bar{\rho}$ that is fixed. Therefore I have anchored the relative air-density error to mean perigee height h_P .

7.1 Propagation of State Estimate

Let $\hat{D}_{n|m}$ denote an optimal estimate of $D(t_n)$, where t_n is the epoch for $\hat{D}_{n|m}$ and t_m is the time of last measurement. Then according to Sherman's Theorem [6][7][9]:

$$\hat{D}_{n|m} = E \{D(t_n) | y_m\} \quad (18)$$

Apply Eq. 18 to Eq. 12, where y_k at time t_k was the last measurement processed:

$$\hat{D}_{k+1|k} = \Phi(t_{k+1}, t_k) \hat{D}_{k|k} \quad (19)$$

Eq. 19 is the filter state estimate propagation equation for the filter time update. Given measurement y_{k+1} at time t_{k+1} use Kalman's filter measurement update theorem, derived from application of Eq. 18 to $D(t_{k+1})$, for the representation:

$$\hat{D}_{k+1|k+1} = E \{D(t_{k+1}) | y_{k+1}\} \quad (20)$$

Propagation of $\hat{D}_{k+1|k+1}$ to time t_{k+2} :

$$\hat{D}_{k+2|k+1} = \Phi(t_{k+2}, t_{k+1}) \hat{D}_{k+1|k+1}$$

7.2 State Estimate Error

Define the error in $\hat{D}_{n|m}$ by:

$$\delta\hat{D}_{n|m} = D_n - \hat{D}_{n|m} \quad (21)$$

Insert Eqs. 19 and 12 into Eq. 21:

$$\delta D_{k+1|k} = \Phi(t_{k+1}, t_k) \delta D_{k|k} + \sqrt{1 - \Phi_{k+1,k}^2} w_k \quad (22)$$

7.3 Base-Line Process Noise Model for Filter Time Update

Square Eq. 22 and apply the expectation operator to get:

$$E \{(\delta D_{k+1|k})^2\} = \Phi^2(t_{k+1}, t_k) E \{(\delta D_{k|k})^2\} + (1 - \Phi_{k+1,k}^2) \sigma_w^2 \quad (23)$$

Notice that:

$$E \{(\delta D_{k|k})^2\} < \sigma_w^2 \quad (24)$$

due to the processing of measurements by the optimal filter. Thus the stochastic sequence defined by Eq. 22 is not stationary.

7.3.1 Baseline Algorithm

The second term in the right-hand side of Eq. 23 is the base-line process noise covariance for deweighting prior estimates of D :

$$q_{k+1,k}^{\Delta\rho/\rho} = (1 - \Phi_{k+1,k}^2) \sigma_w^2 \quad (25)$$

Refer to $[t_k, t_{k+1}]$ as the propagation time interval. For long propagation time intervals the factor $(1 - \Phi_{k+1,k}^2)$ tends to unity, and so $q_{k+1,k}^{\Delta\rho/\rho}$ tends to σ_w^2 . For short propagation time intervals the factor $(1 - \Phi_{k+1,k}^2)$ tends to zero, and so $q_{k+1,k}^{\Delta\rho/\rho}$ tends to zero. Thus the factor $(1 - \Phi_{k+1,k}^2)$ drives the variance $E\left\{(\delta D_{k+1|k})^2\right\}$ toward σ_w^2 in the absence of measurements, but adds little or nothing during dense measurements. When mean values $\langle a_P \rangle$ and $\langle F_{10} \rangle$ are experienced, this is appropriate for the base-line Gauss-Markov model.

But when a_P and F_{10} are much larger than $\langle a_P \rangle$ and $\langle F_{10} \rangle$, then an important model extension is called for. The Gauss-Markov sequence must be immediately interrupted to open the filter gain, particularly during dense measurements.

7.4 Dynamic Process Noise Model for Filter Time Update

The J71 atmospheric density model $\bar{\rho}$ is a function of several arguments. It will suffice here to write:

$$\bar{\rho} = \bar{\rho}(h, F_{10}, \bar{F}_{10}, a_P, t_{k+1}) \quad (26)$$

Define the unitless ratio:

$$R = \frac{\bar{\rho}(h_P, F_{10}, \bar{F}_{10}, a_P, t_{k+1})}{\bar{\rho}(h_P, \langle F_{10} \rangle, \langle F_{10} \rangle, \langle a_P \rangle, t_{k+1})} \quad (27)$$

Define and initialize R_{\max} :

$$R_{\max} = 1 \quad (28)$$

Define and set ϵ to an appropriate small constant positive value. The value of ϵ quantifies what is meant by the least *significant increase* in atmospheric density at perigee height.

7.4.1 Dynamic Algorithm

If $R > R_{\max} + \epsilon$, set $R_{\max} = R$ and define:

$$Q_{k+1,k}^{\Delta\rho/\rho} = R^2 \sigma_w^2 \quad (29)$$

else, set $R_{\max} = R$ and define:

$$Q_{k+1,k}^{\Delta\rho/\rho} = q_{k+1,k}^{\Delta\rho/\rho} \quad (30)$$

Use $Q_{k+1,k}^{\Delta\rho/\rho}$ for air-density error process noise covariance deweighting. Effect: When $\bar{\rho}$ is increasing at h_P due to $F_{10.7}$, $\bar{F}_{10.7}$, and a_P , then the air density variance and filter gain are immediately opened to enable tracking measurements to estimate significant increases in atmospheric density. But when $\bar{\rho}$ is decreasing at h_P due to $F_{10.7}$, $\bar{F}_{10.7}$, and a_P , then the air density variance and filter gain begin their return to the baseline model.

8 Baseline Transform From Perigee Height to Spacecraft Height

Recall Eqs. 6 and 4 to write:

$$\frac{\sigma_{\Delta\rho}(h)}{\bar{\rho}(h)} = f(h) \frac{f(h_P)}{f(h_P)} = \frac{f(h)}{f(h_P)} f(h_P) = \frac{f(h)}{f(h_P)} \frac{\sigma_{\Delta\rho}(h_P)}{\bar{\rho}(h_P)} \quad (31)$$

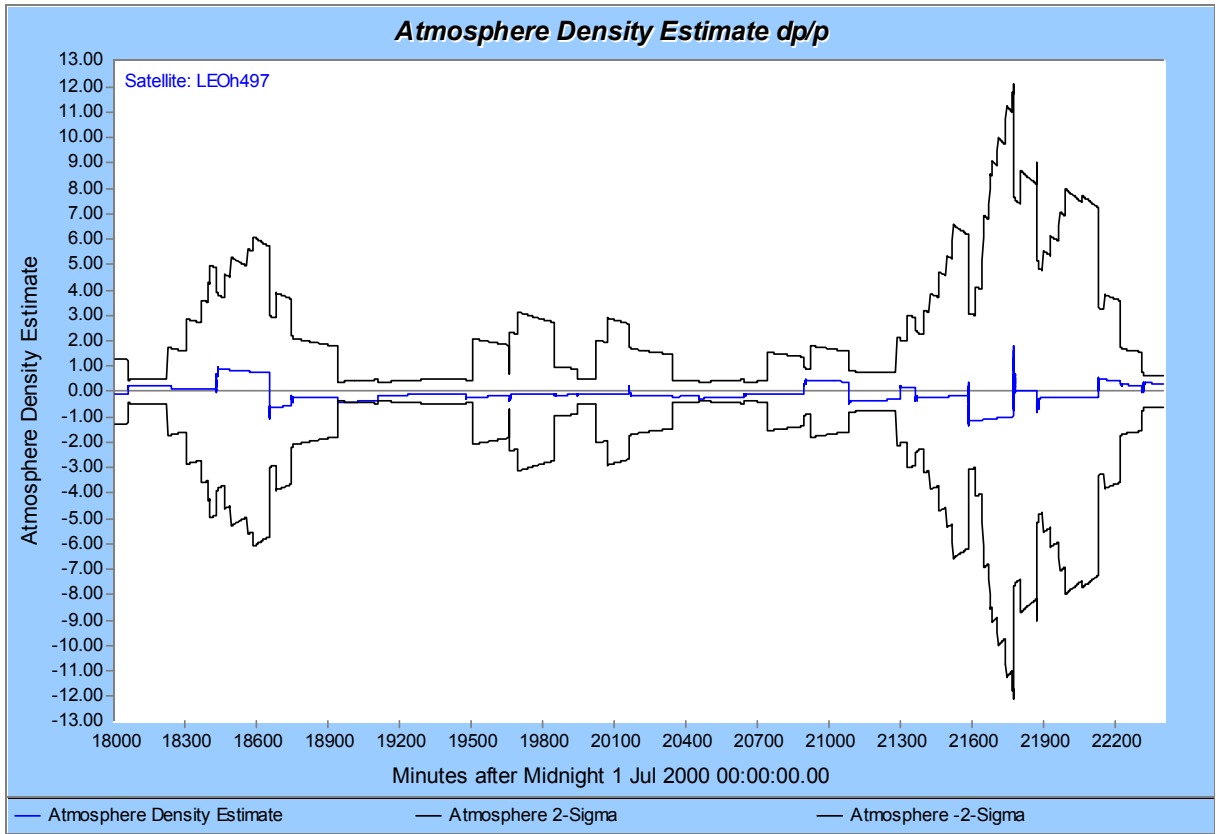


Figure 3: Filtered Atmospheric Density Estimates

Eq. 31 can be derived from:

$$\frac{\Delta\rho(h)}{\bar{\rho}(h)} = \frac{f(h)}{f(h_P)} \frac{\Delta\rho(h_P)}{\bar{\rho}(h_P)} \quad (32)$$

which, with the aid of Eq. 11, can be written:

$$D(h) = \frac{f(h)}{f(h_P)} D(h_P) \quad (33)$$

From Eq. 5:

$$\begin{aligned} \rho(h) &= \bar{\rho}(h) + \Delta\rho(h) \\ &= \bar{\rho}(h) \left[1 + \frac{\Delta\rho(h)}{\bar{\rho}(h)} \right] \end{aligned} \quad (34)$$

Insert Eq. 32 into Eq. 34:

$$\rho(h) = \bar{\rho}(h) \left[1 + \frac{f(h)}{f(h_P)} \frac{\Delta\rho(h_P)}{\bar{\rho}(h_P)} \right]$$

and apply Sherman's Theorem to get:

$$\hat{\rho}(h) = \bar{\rho}(h) \left[1 + \frac{f(h)}{f(h_P)} \frac{\Delta\hat{\rho}(h_P)}{\bar{\rho}(h_P)} \right]$$

or:

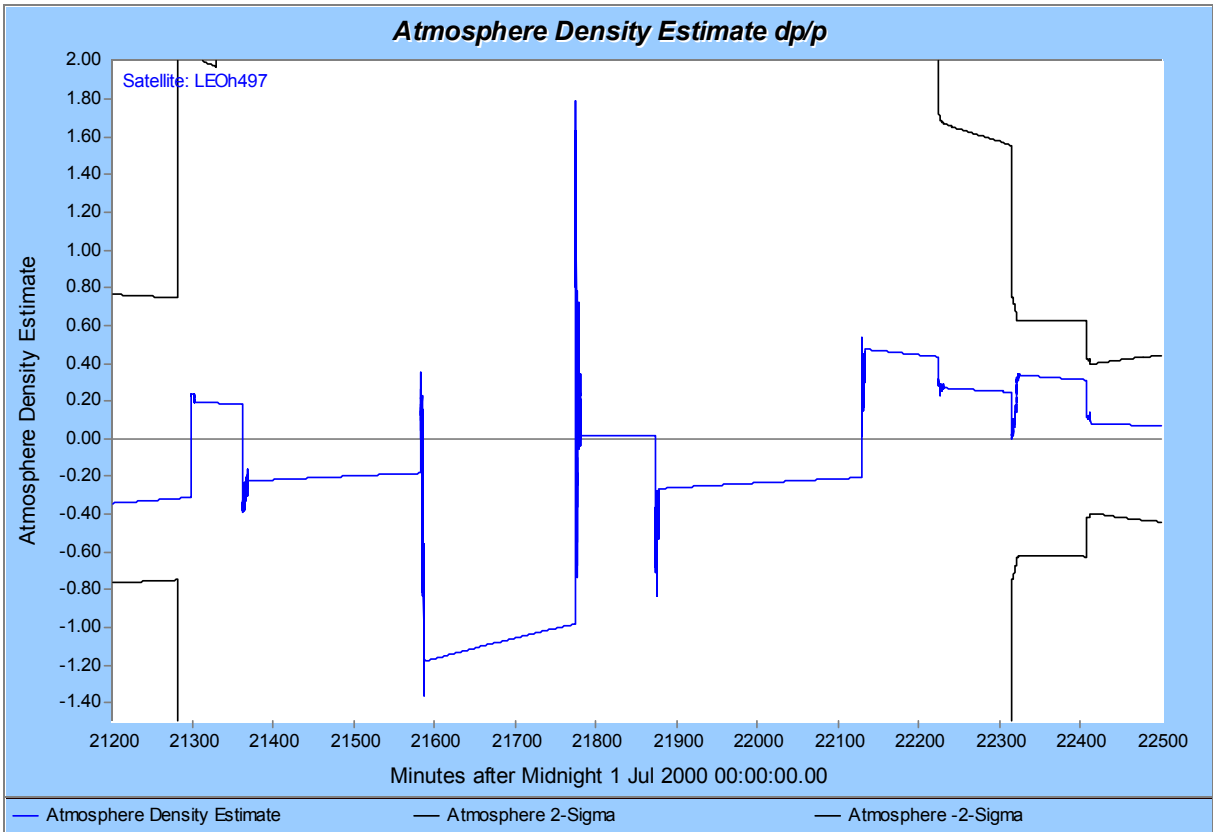


Figure 4: Filtered Geomagnetic Response to CME

$$\hat{\rho}(h) = \bar{\rho}(h) \left[1 + \frac{f(h)}{f(h_P)} \hat{D}(h_P) \right] \quad (35)$$

Eq. 35 defines my method to map the filter estimate \hat{D} at perigee height h_P to the estimate $\hat{\rho}(h)$ of atmospheric density, at current height h , for use in trajectory propagation.

8.1 Discussion

The baseline height transformation factor $f(h)/f(h_P)$ is used in Eq. 32, as well as in Eq. 31, to guarantee consistency between the height dependent *stochastic error* transform model and the height dependent *error estimate* transform model for atmospheric density. This frees the height transform from wild perturbations that would be suffered due to the use of local time-constants and discontinuities in $F_{10.7}$ and a_P , and provides stability to the estimate $\hat{D}(h_P)$ at perigee height. The spacecraft does sample its own perigee height once per orbit, and perigee height is most significant with respect to atmospheric density modeling errors.

9 Real Data Results

The new method for real-time atmospheric density estimation has been implemented and tested in STK/OD⁴ with simulated tracking data and real tracking data. The figures for real data results display atmospheric density estimation response to range tracking data, from fourteen ground stations, to two spacecraft in LEO. The sequential filter began processing range data early on 1 July 2000,

⁴A new orbit determination product from Analytical Graphics, Inc.

and terminated late on 26 July 2000 due to the beginning of a six day gap in the archived tracking data.

$F_{10.7}$ began with 163.7 on 1 July, had a global peak at 314.6 on 12 July, receded to 203.9 on 14 July, had a minor peak of 261.9 on 18 July, and receded to 174.6 on 26 July.

a_P began with 4.0 on 1 July, had a global peak of 400.0 at 18^h on 15 July, and experienced ten other minor peaks during the 26 day July interval.

The abscissa (X Axis) for each figure is given in units of minutes after 1 July 2000 0^h UTC, denoted hereafter as MAE (Minutes After Epoch). The ordinate (Y Axis) for each figure presents the change in atmospheric density relative to J71. The time varying estimate of relative atmospheric density $\Delta\hat{\rho}/\bar{\rho}$ is displayed in blue, and the associated $\pm 2\sigma$ error envelope is displayed in black. Each unit on the ordinate is associated with a 100% change in atmospheric density.

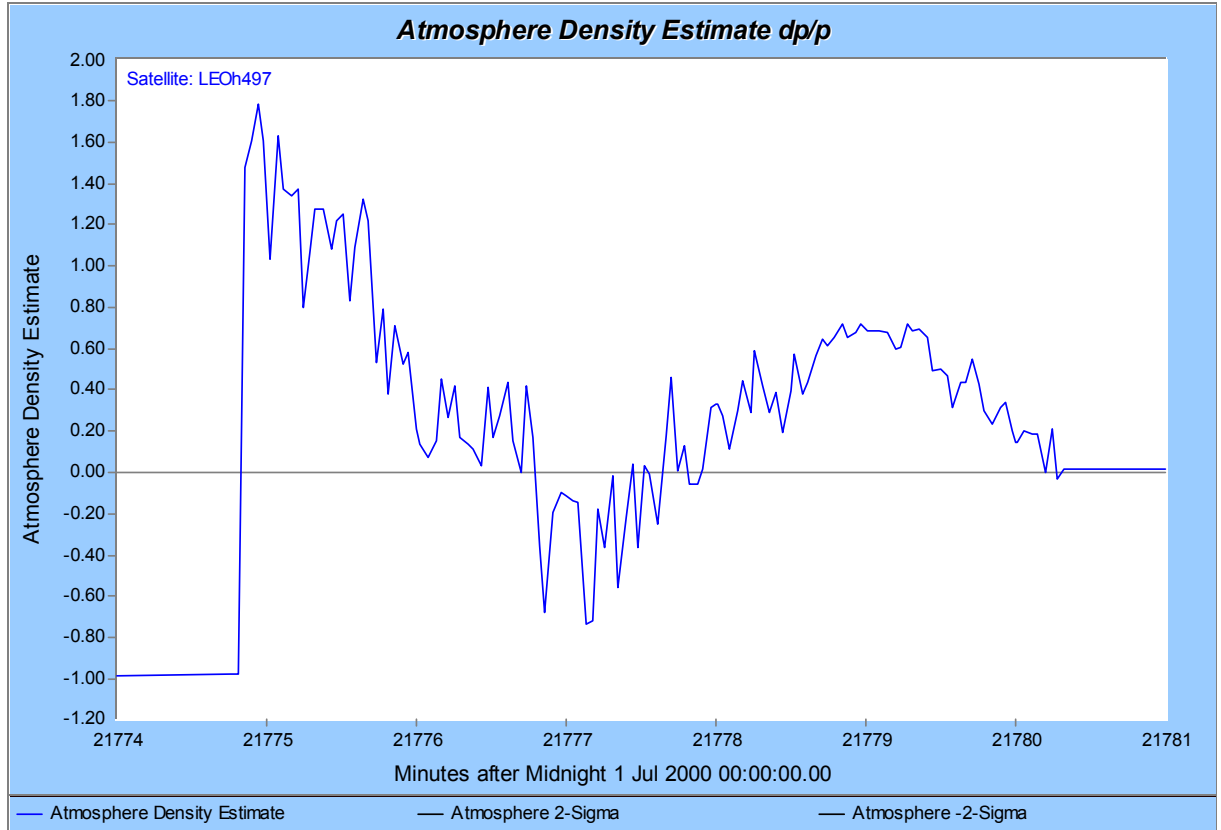


Figure 5: Filter Response to Range Measurements at Geomagnetic Peak

9.1 Filter Update Functions

The sequential filter performs time update and measurement update functions recursively. The time update function has two vital activities: (1) It accumulates atmospheric density error variance with time, and (2) It propagates the atmospheric density estimate and its error variance across time intervals between measurements. Time intervals between station passes are long, and time intervals between range measurements within each station pass are short. The Gauss-Markov exponential half-life used by the filter sends the estimate (blue line) toward zero, in these time intervals, at a rate defined by the value used for half life. Here the exponential half life constant was set to 700 minutes.

It is important to note that significant step changes in modeled atmospheric density are induced by changes in $F_{10.7}$, $\bar{F}_{10.7}$, and a_P according to J71. These changes are always *wrong* because

they are modeled as time constants, and have significant fictitious discontinuities at time constant boundaries, as discussed above. The associated errors in $F_{10.7}$ or a_P may thus be positive or negative.

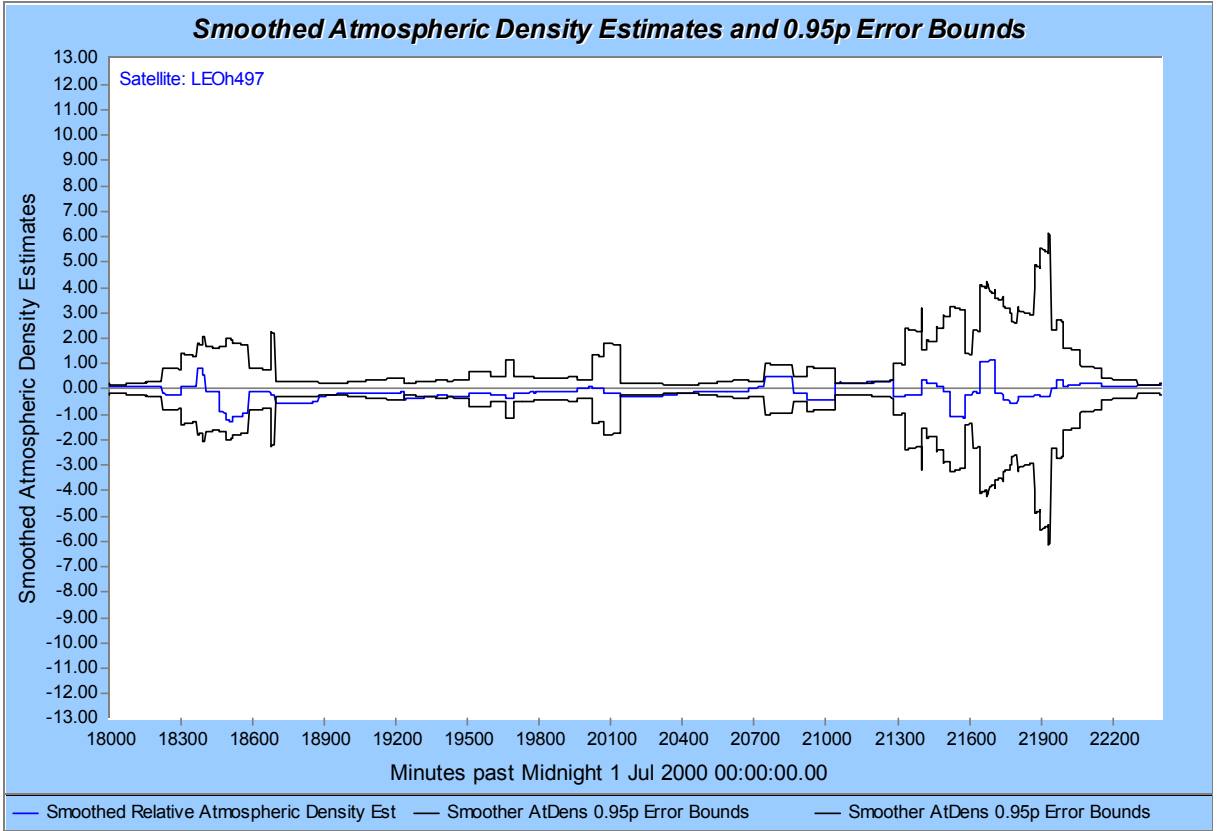


Figure 6: Smoothed Atmospheric Density Estimates

Each significant step change in the sequential atmospheric density estimate is associated with the commencement of range tracking data⁵ processing by the filter measurement update function after a long time interval between station passes. These step changes may be positive or negative because the associated atmospheric density errors may be positive or negative.

9.2 LEO $h = 497km$

9.2.1 Sequential Filter

Fig. 3 displays the filter response to range data from 13 July 2000 12^h 0^m (18000 MAE) through 16 July 2000 13^h 20^m (22400 MAE). The filter was initialized on 1 July 2000 0^h. The baseline error variance model is clearly distinguished here from the dynamic error variance model.

The large positive step in the estimate at approximately MAE 18400 (13 July 2000 18^h 42^m) is correlated with a peak of $F_{10.7} = 314.6$ for 12 July 2000. This is the global peak in $F_{10.7}$ across the entire July interval. The Jacchia defined $F_{10.7}$ lag for the direct solar effect on atmospheric density is 1.70 days, or 40.8 hours. This corresponds to the interval from 16.8 hours on 13 July 2000 to 16.8 hours on 14 July 2000.

It is significant to note that the global peak in a_P follows, and is clearly detached from, the global peak in $F_{10.7}$. The global peak in a_P is associated with the largest estimate magnitudes for atmospheric density across the entire processing interval.

⁵It would be preferable to process dense GPS range and/or Doppler data completely around the orbit so as to reduce or eliminate this step change.

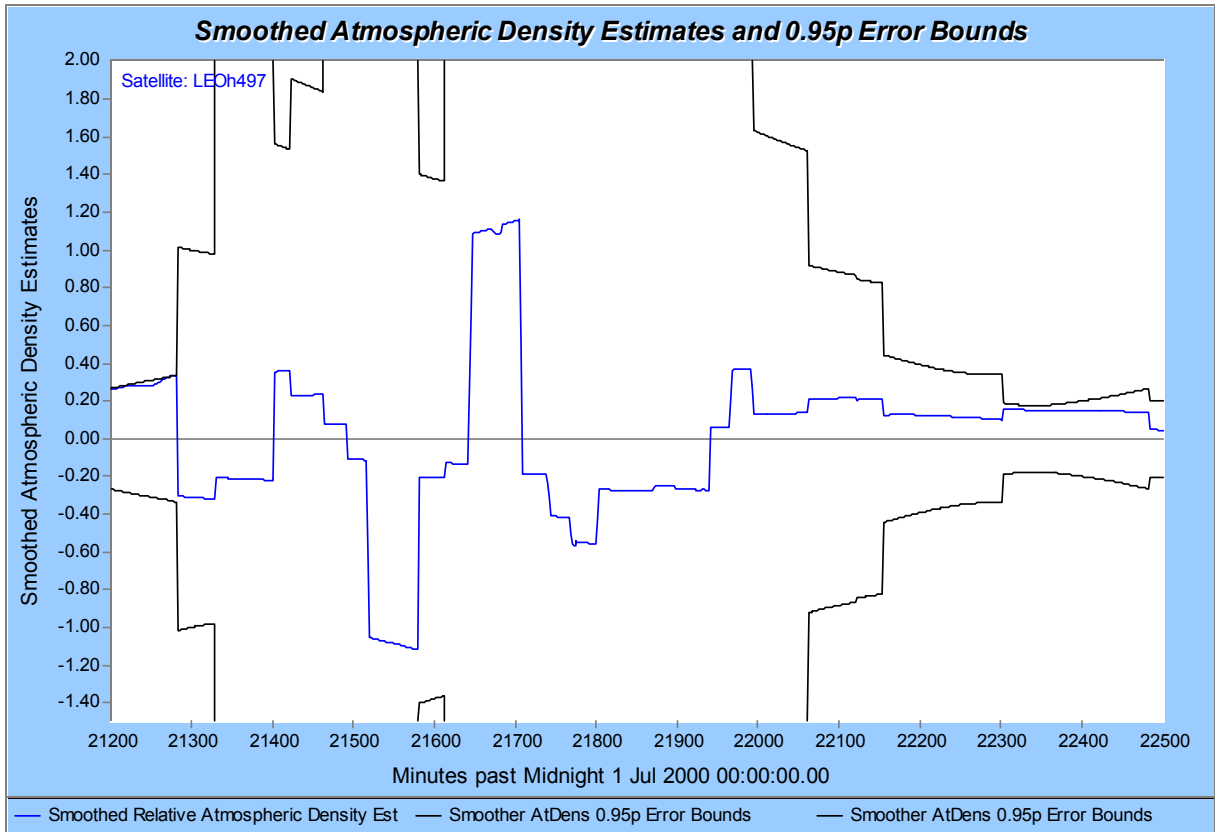


Figure 7: Smoothed Geomagnetic Response to CME

Fig. 4 displays the filter response, between MAE 21200 and MAE 22500. These times are associated with 15 July 2000 17^h 20^m and 16 July 2000 15^h 0^m respectively. The peak STK/OD filtered estimate in atmospheric density is seen to be about 1.8 (180%), of the density modeled by J71, at approximately 16 July 2000 2.92 hours.

The $a_P = 400$ peak occurs on 15 July 2000 across the interval (18, 21) hours. The Jacchia defined a_P lag for the geomagnetic effect on atmospheric density is 0.279 days, or 6.696 hours. Then the *effect* of the $a_P = 400$ peak on atmospheric density occurs on 16 July 2000 across the interval (0.696, 3.696) hours. Note that the peak STK/OD estimate in atmospheric density falls within this interval, but that most of the four minute positive estimate sequence lies to the right of interval (0.696, 3.696) hours.

Fig. 5 magnifies the effective a_P peak on 16 July 2000 2.92 hours, and shows the detailed response to filtering range measurements.

9.2.2 Sequential Smoother

Fig. 6 displays the filter-smoother response to range data from 13 July 2000 12^h 0^m (18000 MAE) through 16 July 2000 13^h 20^m (22400 MAE). It is scaled as the filtered response of Fig. 3 so as to enable easy comparison.

The filter responds only to range data prior to the time of response, whereas the smoother responds to range data both prior to and after the time of response. The smoothed estimate uses more local information than the filtered estimate. It is thus not surprising that smoothed estimates and root-variances are smaller than those from the filter. But the filtered estimate function has been reshaped by the smoother.

Fig. 7 focuses the smoother response on the CME interval, between MAE 21200 and MAE 22500, and is comparable to the filtered response of Fig. 4. The *effective* $a_P = 400$ peak on atmospheric

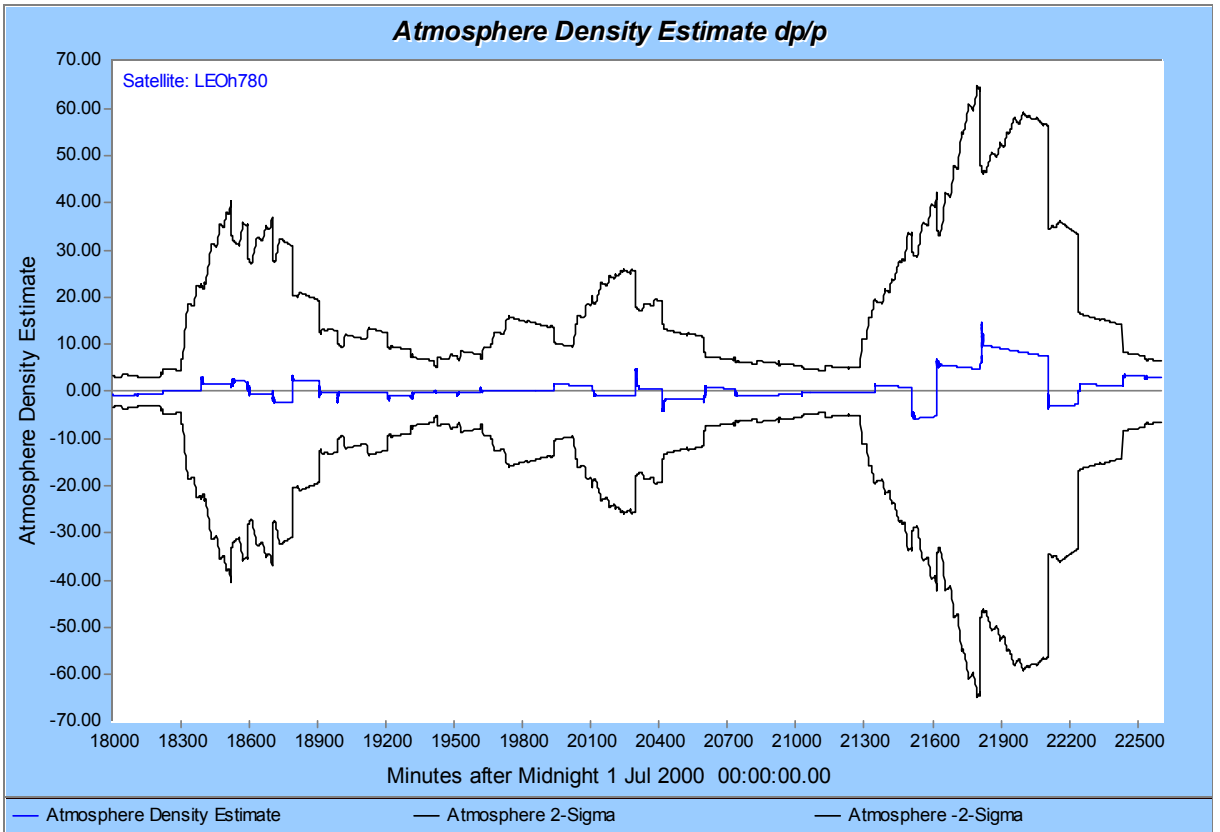


Figure 8: Filtered Atmospheric Density Estimates

density occurs on 16 July 2000 across the interval (0.696, 3.696) hours. Note that the entire one hour smoothed estimate peak in atmospheric density falls within this interval. The smoother has shifted the filtered estimate function to the left by 110 minutes (bringing it entirely within the interval predicted by Jacchia), has reshaped it, and has reduced the filtered peak from 1.8 to less than 1.2.

9.3 LEO $h = 780km$

9.3.1 Sequential Filter

Fig. 8 displays the filter response to range data from 13 July 2000 12^h 0^m (18000 MAE) through 16 July 2000 16^h 40^m (22600 MAE). The filter was initialized on 1 July 2000 0^h. The baseline error variance model is not so clearly distinguished from the dynamic error variance model.

The large positive step in the estimate at approximately MAE 18400 (13 July 2000 18^h 42^m) is correlated with a peak of $F_{10.7} = 314.6$ for 12 July 2000. This is the global peak in $F_{10.7}$ across the entire July interval. The Jacchia defined $F_{10.7}$ lag for the direct solar effect on atmospheric density is 1.70 days, or 40.8 hours. This corresponds to the interval from 16.8 hours on 13 July 2000 to 16.8 hours on 14 July 2000.

The step at 18400 MAE of Fig. 8 is correlated with a peak of $F_{10.7} = 314.6$ for 12 July 2000. This is the global peak in $F_{10.7}$ across the entire July interval. 18400 MAE is associated with 18.7 hours on 13 July 2000. The Jacchia defined $F_{10.7}$ lag for the direct solar effect on atmospheric density is 1.70 days, or 40.8 hours. This corresponds to the interval from 16.8 hours on 13 July 2000 to 16.8 hours on 14 July 2000.

Fig. 9 displays the filter response, between MAE 21200 and MAE 22600. These times are associated with 15 July 2000 17^h 20^m and 16 July 2000 16^h 40^m respectively. The peak STK/OD filtered estimate in atmospheric density is seen to be about 14.7 (1470%), of the density modeled by

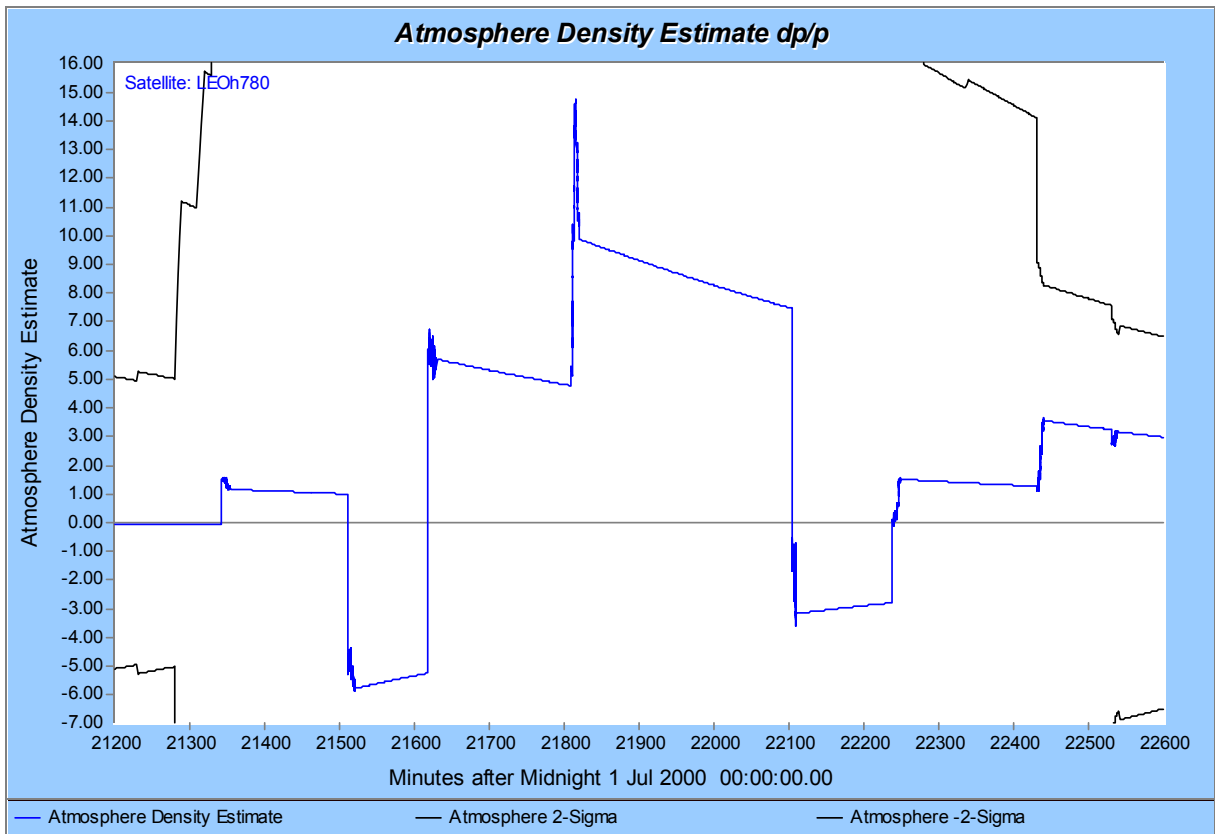


Figure 9: Filtered Geomagnetic Response to CME

J71, at approximately 16 July 2000 $3^h 40^m$.

The $a_P = 400$ peak occurs on 15 July 2000 across the interval (18, 21) hours. The Jacchia defined a_P lag for the geomagnetic effect on atmospheric density is 0.279 days, or 6.696 hours. Then the *effect* of the $a_P = 400$ peak on atmospheric density occurs on 16 July 2000 across the interval (0.696, 3.696) hours. Note that the peak STK/OD estimate in atmospheric density falls within this interval.

Fig. 10 displays the filtered response to range measurements for the peak at 21816 MAE (16 July 2000 $3^h 36^m$).

9.3.2 Sequential Smoother

Fig. 11 displays the filter-smoother response to range data from 13 July 2000 $12^h 0^m$ (18000 MAE) through 16 July 2000 $13^h 40^m$ (22600 MAE). It is scaled as the filtered response of Fig. 8 so as to enable easy comparison.

Fig. 12 magnifies the smoothed response between 15 July 2000 $17^h 20^m$ (MAE 21200) and 16 July 2000 $16^h 40^m$ (MAE 22600). The filtered peak in the atmospheric density estimate is reduced by the smoother from 14.7 to 10.0, is shifted to the left by about 50 minutes, and is broadened and reformed.

9.4 The Smoother Shift to the Left

The peak filtered estimate in atmospheric density was shifted to the left by the smoother for both *LEOh497* and *LEOh780*. The following explanation is offered.

Range measurements sit in position space, two time-integrals above the air-drag accelerations. These integrals are time lags. Thus the sensing of atmospheric density from range measurements by

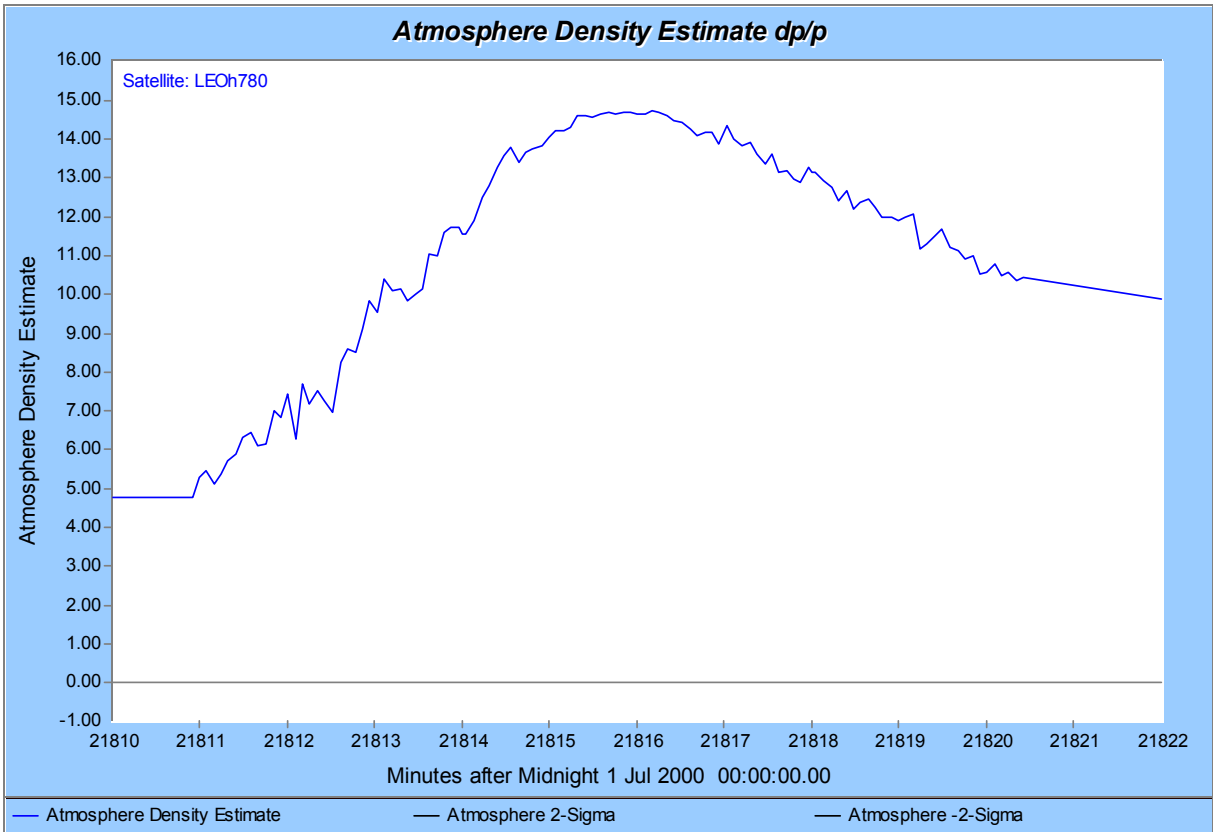


Figure 10: Filter Response to Range Measurements at Geomagnetic Peak

the filter lags the time of actual change in the atmospheric density.

The optimal filtered estimate is derived only from information that sits to the left of the filter epoch. On the other hand, the optimal smoothed estimate is derived from information that sits both to the left *and to the right* of the smoother epoch. This provides the smoother with a significant advantage in estimation of the atmospheric density error function, relative to the filter. Having used information from the right of a peak, and from the right of the integral lag, the smoother is enabled to more accurately estimate the atmospheric density error function.

9.4.1 Use the Filtered Estimate for Predictions

The last filtered estimate is the first smoothed estimate, and subsequent smoothed estimates are calculated backwards with time. The last filtered estimate is the optimal estimate for use in trajectory prediction. Observable atmospheric density modeling error is absorbed by the atmospheric density error filter state parameter. Otherwise the atmospheric density modeling error would be aliased into the orbit estimate.

10 Optimality Validation

Optimality validation consists in demonstrating that range residuals are white, and that the McReynolds filter-smoother consistency test is satisfied at the 0.99 probability level. The first test is satisfied, and the second test is satisfied most of the time. An explanation for failures in the second test has been identified.

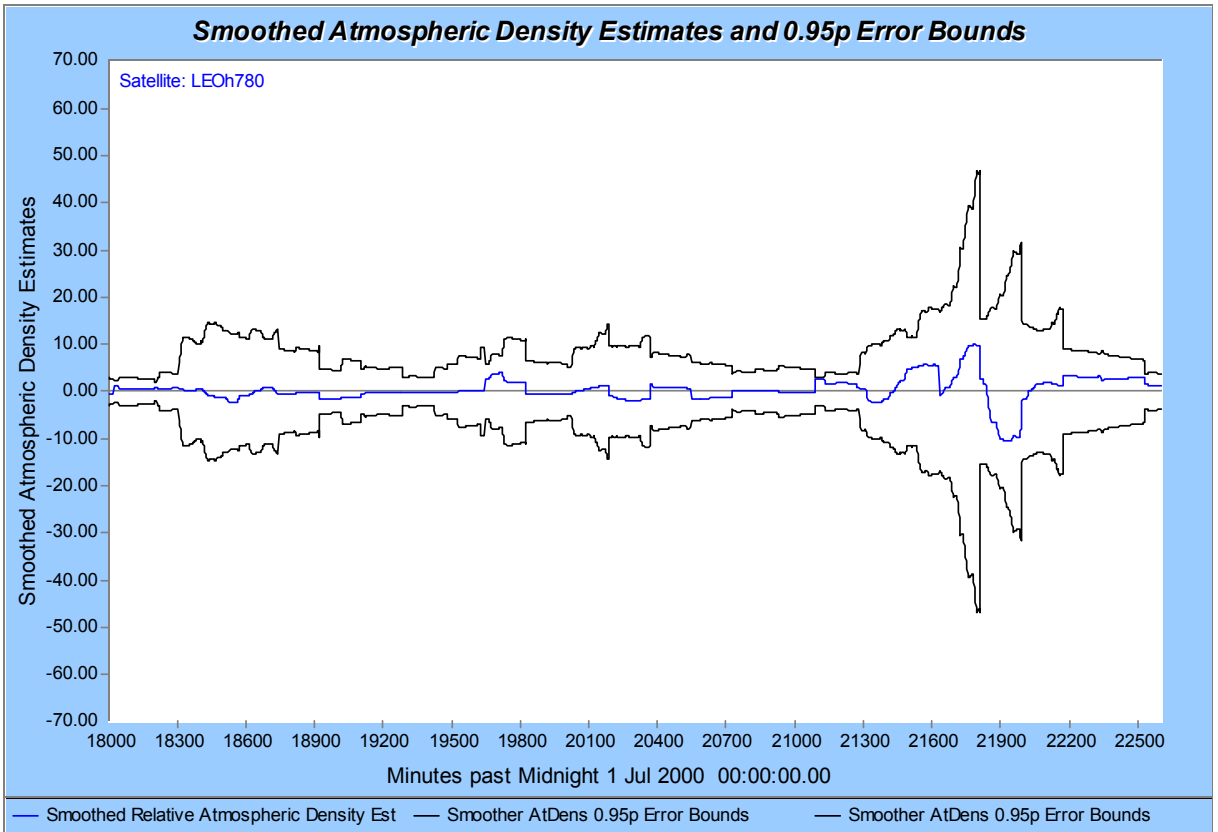


Figure 11: Smoothed Atmospheric Density Estimates

10.1 White Noise Range Residuals

Inspection of range residual graphics shows consistency with white noise.

10.2 McReynolds' Filter-Smoother Consistency Test

Inspection of filter-smoother consistency test graphics shows consistency most of the time. However there are time intervals during which this test clearly fails. These failures have been identified to coincide with the commencement of range data, after long prediction time intervals, when filtered atmospheric density estimates make very large corrections. These failures would be eliminated by taking tracking data densely about the orbit; e.g., by using an onboard GPS receiver.

11 Summary

Using real range tracking data at solar maximum for two spacecraft in LEO, the new method for real-time estimation of atmospheric density has been shown to estimate significant time-varying corrections to local atmospheric density that are closely correlated in time to the *effective* times for observed values of both $F_{10.7}$ and a_P . Atmospheric density is demonstrated to be consistently driven by significant disturbances in the geomagnetic field. The atmospheric density estimation algorithm has new features:

- *Sequential* processing of range and/or Doppler measurements using an optimal filter-smoother
- Simultaneous estimation of local atmospheric density for multiple spacecraft

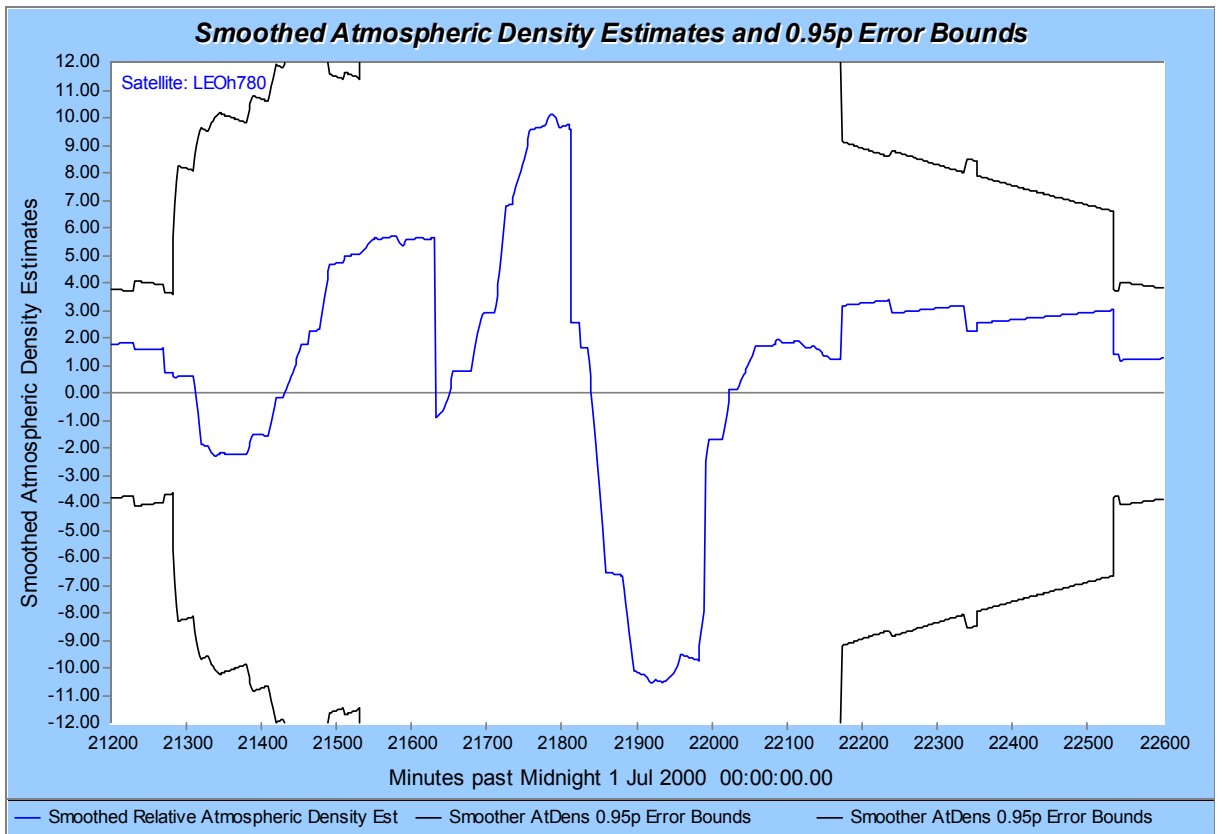


Figure 12: Smoothed Geomagnetic Response to CME

- Use of the historical record on $F_{10.7}$ and a_P to define a baseline stochastic atmospheric density error model
- Use of current values of $F_{10.7}$ and a_P to define a dynamic stochastic atmospheric density error model

12 Real-Time Global Atmospheric Density Estimation

Looking forward, it is appropriate to consider again[14] the sequential real-time *global* estimation of atmospheric density. What is the relation between *local* and *global* estimation of atmospheric density?

Given tracking measurements from an ensemble of LEO spacecraft, consider global estimation without local estimation. Then locally there would always exist significant *observable* atmospheric density modeling errors. But by definition, optimal orbit determination[11] requires that every unknown observable effect must have a place in the state estimate structure. Therefore local estimation is required *simultaneously* with global estimation.

In 1990 I proposed[14] the transformation of appropriate parameter time constants in J71 to serially correlated stochastic parameter sequences. The stochastic parameters were to be estimated in real time, their error variances were to be constant (stationary) during propagation, and reduced appropriately due to measurements. This part of the 1990 proposal is proposed again.

13 Acknowledgements

13.1 Tom Gidlund

Tom Gidlund [18], with U. S. Air Force support, provided a substantial sequence of real range and Doppler tracking data from two LEOs at solar maximum, from the summer of year 2000, for use in the validation of our new sequential orbit determination method STK/OD. The LEO orbits are near circular, and are separated in height by roughly $280km$. The effects of a huge coronal mass ejection impacted the earth's geomagnetic field with a_P rising to 400 at 18^h on 15 July, where $F_{10.7}$ had peaked at 314.6 on 12 July. This provided two very useful LEO test cases.

This tracking data was also used in the development of our new *baseline and dynamic atmospheric density error models*. The separation in height of the two LEOs presented useful cases in relating volatile changes in atmospheric density to specification of filter process noise error variance at significantly different spacecraft heights.

13.2 Hujsak, Cottam, and Pechenick

Dependence of our new *baseline atmospheric density error model* on the historical record of $F_{10.7}$ and a_P was first suggested by Richard Hujsak [17]. A related study was assigned to Russ Cottam and Kay Pechenick under ATA contract to AFSPACECOM in 1986. Unfortunately the AFSPACECOM contract was cancelled before an atmospheric density error model could be completed, applied, or demonstrated.

13.3 Analytical Graphics, Inc.

Conversion of the MACH 10 prototype to STK/OD was performed by members of the AGI development team, especially Kevin O'Brien, Jim Woodburn, Jim Fields, Matt Amato, Kevin Murray, Jeff Gassert, Jim Wilson, Dave Holland, and Ralph Patrick. I wish to thank Paul Graziani for his patient and sustained support during my development of the MACH 10 prototype.

References

- [1] L. G. Jacchia, *Revised Static Models of the Thermosphere and Exosphere with Empirical Temperature Profiles*, Smithsonian Astrophysical Observatory, Special Report 332, 1971
- [2] The Committee for the CIRA Working Group 4, *COSPAR International Reference Atmosphere 1972 (CIRA 1972)*, Akademie-Verlag, Berlin, 1972
- [3] L. G. Jacchia, *New Static Models of the Thermosphere and Exosphere with Empirical Temperature Profiles*, Smithsonian Astrophysical Observatory, Special Report 313, 1970
- [4] L. G. Jacchia, *Thermospheric Temperature, Density, and Composition: New Models*, Smithsonian Astrophysical Observatory, SAO Special Report 375, 1977
- [5] Sherman, S., *A Theorem on Convex Sets with Applications*, Ann. Math. Stat., 26, 763-767, 1955.
- [6] Sherman, S., *Non-Mean-Square Error Criteria*, IRE Transactions on Information Theory, Vol. IT-4, 1958.
- [7] Kalman, R. E., *New Methods in Wiener Filtering Theory*, Proceedings of the First Symposium on Engineering Applications of Random Function Theory and Probability, edited by J. L. Bogdanoff and F. Kozin, John Wiley & Sons, New York, 1963.
- [8] Rauch, H. E., *Solutions to the Linear Smoothing Problem*, IEEE Trans. Autom. Control, vol. AC-8, p. 371, 1963
- [9] Meditch, J. S., *Stochastic Optimal Linear Estimation and Control*, McGraw-Hill, New York, 1969.

- [10] J. K. Owens, *NASA Marshall Engineering Thermosphere Model – Version 2.0*, NASA/TM-2002-211786, June 2002, Section 3.2.3 Geomagnetic Activity: "Although high-latitude ionospheric current fluctuations drive the magnetic field fluctuations observed at these stations, the magnetic field fluctuations do not drive the thermosphere."
- [11] James R. Wright, *Optimal Orbit Determination*, Paper AAS02-192, AAS/AIAA Space Flight Mechanics Meeting, San Antonio, Texas, 27-30 January, 2002
- [12] James R. Wright, *Sequential Orbit Determination with Auto-Correlated Gravity Modeling Errors*, AIAA, Journal of Guidance and Control, Vol 4, No. 2, May-June 1981, page 304.
- [13] James R. Wright, *Orbit Determination Solution to the Non-Markov Gravity Error Problem*, AAS/AIAA Paper AAS 94-176, AAS/AIAA Spaceflight Mechanics Meeting, Cocoa Beach, FLA, Feb., 1994.
- [14] James R. Wright, *Near Real Time Atmospheric Density Estimation*, Applied Technology Associates, Inc. (ATA), 11 August 1990. This informal ATA company paper proposed a near real time global method for estimation of atmospheric density.
- [15] James L. Burch, *The Fury of Space Storms*, Scientific American, April 2001, page 86.
- [16] Meditch, J. S., Personal Communications, 1974. A private lecture on the importance of Sherman's Theorem
- [17] Richard Hujsak, Personal Communications, 1980-1996.
- [18] Tom Gidlund, Personal Communications, 2000-2001.
- [19] L. G. Jacchia, Personal Communication via telecom, 1978